A numerical matching technique for linear resistive magnetohydrodynamics modes

M. Furukawa,[1,a)] S. Tokuda,[2] and L.-J. Zheng[3]
[1]*Graduate School of Frontier Science, University of Tokyo, 5-1-5 Kashiwanoha, Kashiwa-shi, Chiba 277-8561, Japan*
[2]*Research Organization for Information Science and Technology, Tokai-mura, Ibaraki 319-1106, Japan*
[3]*Institute for Fusion Studies, University of Texas at Austin, Austin, Texas 78712, USA*

(Received 11 December 2009; accepted 9 April 2010; published online 13 May 2010)

A new numerical matching technique for linear stability analysis of resistive magnetohydrodynamics (MHD) modes is developed. The solution to the resistive reduced MHD equations in an inner layer with a finite width is matched onto the solution to the inertialess ideal MHD or the Newcomb equation by imposing smooth disappearance of parallel electric field in addition to the continuity of perturbed magnetic field and its spatial gradient. The boundary condition for the parallel electric field is expressed as a boundary condition of the third kind for the stream function of the perturbed velocity field. This technique can be applied for the reversed magnetic shear plasmas of their minimum safety factors being rational numbers, for which the conventional asymptotic matching technique fails. In addition, this technique resolves practical difficulties in applying the conventional asymptotic matching technique, i.e., the sensitivity of the outer-region solution on the accuracy of the local equilibrium as well as the grid arrangements, even in normal magnetic shear plasmas. Successful applications are presented not only for the eigenvalue problem but also for the initial-value problem. © *2010 American Institute of Physics*.
[doi:10.1063/1.3420244]

I. INTRODUCTION

Asymptotic matching technique is one of the principal methods for linear stability analysis of resistive magnetohydrodynamics (MHD) modes such as tearing modes.[1,2] So far a number of applications have been made on the stability calculations of plasmas with cylindrical[3–7] and toroidal geometries.[8–11]

In applying the asymptotic matching method, the plasma region is divided into two kinds of regions: a thin inner layer around the mode-resonant surface and ideal MHD regions except for the layer. Plasma inertia and resistivity are retained only in the inner layer since the field-line bending term becomes vanishingly small around the mode-resonant surface. In the ideal MHD region, on the contrary, the inertialess ideal MHD equation or the Newcomb equation is solved.[12,13] The Newcomb equation has a regular singular point at the mode-resonant surface if the magnetic shear does not vanish there. Thus, the Newcomb equation has square-integrable (small) and non-square-integrable (big) solutions. In order to match the solution for the ideal MHD region onto the solution for the inner layer, the ratio of the small solution to the big solution, or the so-called matching data, plays a crucial role. However, the big solution dominates the small solution as getting closer to the mode-resonant surface and it becomes difficult to accurately capture the matching data numerically. Highly sophisticated theory has been developed so far for cylindrical[5,7] and toroidal geometries.[9,11,14,15] Even if we utilize such theory, the matching data have been revealed to be sensitive to local MHD equilibrium accuracy and grid arrangements at the mode-resonant surface by numerical experiments.[14] In addition, the Frobenius series solution is possible only if the mode-resonant surface is a regular singular point. If the magnetic shear vanishes at the mode-resonant surface, it becomes an irregular singular point, and therefore the above argument fails from the beginning.

In the inner layer, on the other hand, the governing equations are simplified considerably since the equilibrium quantities such as magnetic field are approximated to be linearly varying in the radial coordinate, although plasma inertia and resistivity are retained.[1,2,16] Careful treatment is also required for this inner-layer equation since it has irregular singular points at infinity and the solution has an infinite norm.[2,11,17] The response formalism[5] has been adopted to resolve this problem and was successfully applied to an initial-value problem.[11,18]

In the present paper, we propose a new method for computing the linear stability of resistive MHD modes via matching technique, where the plasma region is divided into ideal MHD regions and an inner region with *finite width*. Asymptotic solutions around the mode-resonant surface are not used in our numerical matching technique. The advantages to use the inner region with finite width are as follows. The most crucial feature is that our numerical matching technique is applicable to reversed magnetic shear plasmas of their minimum safety factors being rational numbers. The conventional asymptotic analysis fails for these cases since the Frobenius series solution of the Newcomb equation used for the asymptotic matching can be obtained only if the mode-resonant surface is a regular singular point as mentioned above. If the mode-resonant surface has the minimum

a)Electronic mail: furukawa@k.u-tokyo.ac.jp.

safety factor in the reversed magnetic shear plasma, then it is an irregular singular point of the Newcomb equation. Secondly, an important feature is related to the sensitivity on the numerical accuracy. It is known that matching data, obtained from the outer solution, are sensitive to the local accuracy of MHD equilibrium and the local grid arrangements around the mode-resonant surface even for normal magnetic shear plasmas.[14,19] Since we will use the inner region with finite width, we do not need to integrate the Newcomb equation so close to the mode-resonant surface. Then the sensitive behavior on the local properties can be fully avoided. Thirdly, there is no irregular singularity in the inner-region equation since the stretched radial coordinate is not used; we do not need to consider infinity in the stretched radial coordinate. Finally, this method can be easily applied to initial-value problems, as shown in Sec. II. This can lead to a study of nonexponential behavior. We also expect that our method can be extended to study weakly nonlinear phenomena. Needless to say, more detailed model equations can be adopted as the inner-region equation, which is one of the advantages to utilize the matching method. Note that the scope of this paper is to develop a method applicable to the simplest linear stability problem, though we expect that this can provide a basis for those future extensions.

In the inner region, the high-beta reduced MHD equation[20,21] is solved. Then the solution is matched onto the solution of the Newcomb equation by using boundary conditions developed in Sec. II C. We will observe good convergence of the solutions to those obtained by solving the resistive reduced MHD equations in the whole plasma region. As we will see, the width of the inner region can be 1% of the minor radius or less for the Lundquist number of 10^{12}, although it, of course, depends on equilibrium parameters such as magnetic shear and the Lundquist number.

The matching technique using an inner region with finite width was originally developed for ideal MHD modes in a cylindrical geometry, and good performance was shown.[19] Recently, it was applied to resistive wall mode stability analysis including toroidal rotation in a cylindrical geometry.[22] Our method extends this idea to resistive MHD modes. The main difficulty in this extension is that the linearized resistive MHD equation has more independent solutions than the linearized ideal MHD equation since the resistivity increases the order of derivatives. Thus, an appropriate set of independent solutions in the inner region needs to be selected when matching onto the solution in the ideal MHD region. In order to resolve this difficulty, we have developed a boundary condition that selects independent solutions suitable for matching onto the solution in the ideal MHD region. As explained in the main text, this boundary condition is imposed on the stream function of the perturbed velocity field and makes the parallel electric field smoothly approach zero.

The present paper is organized as follows. Our numerical matching technique using an inner region with finite width is developed in Sec. II as an eigenvalue problem. Several examples are shown for tearing, internal kink, and resistive interchange modes in normal magnetic shear plasmas and double tearing mode in reversed magnetic shear plasmas. In the normal magnetic shear plasmas, the conventional asymptotic matching theory predicts that the growth rate γ is proportional to $\eta^{3/5}$ for the tearing mode and $\eta^{1/3}$ for the internal kink and resistive interchange modes, respectively, where η is the resistivity. We will show that our numerical matching technique reproduces these η dependence of γ when η is small enough so that the conventional asymptotic matching theory serves as a good approximation. We will also show that our numerical matching technique is also applicable to relatively large η, where the assumption for the conventional theory breaks down and the η dependence deviates from $\eta^{3/5}$ or $\eta^{1/3}$. As for the double tearing mode, we will show that our numerical matching technique is also applicable to the case where the mode-resonant surface becomes an irregular singular point of the Newcomb equation. Next, the application to the initial-value problem is developed in Sec. III. An implicit time-integration scheme is used. In Sec. IV, a discussion is given on the application of the present numerical matching method to the stability calculations of high-beta plasmas in a toroidal geometry. Conclusions are given in Sec. V.

II. LINEAR EIGENVALUE PROBLEM

A. Settings and governing equations

Let us consider a cylindrical finite-beta plasma with a fixed boundary. The cylindrical coordinate system (r,θ,z) is used, and the unit vectors in each direction are $\hat{\mathbf{r}}$, $\hat{\boldsymbol{\theta}}$, and $\hat{\mathbf{z}}$, respectively. Toroidal angle ζ is defined by z/R_0, where $2\pi R_0$ is the length of the plasma column. Perturbed quantities are assumed to have the spatial dependence $e^{i(m\theta+n\zeta)}$, where m and n are the poloidal and toroidal mode numbers, respectively. The plasma minor radius is a. The aspect ratio $A:=R_0/a$ is assumed to be large. The inverse aspect ratio is denoted by $\varepsilon:=1/A$. All the calculation data presented in the following are obtained for $A=10$.

For a case of normal magnetic shear or monotonic safety factor q profile, let us assume that there is a mode-resonant surface at $r=r_s$ inside the plasma region. For a case of reversed q profile, we assume that the minimum safety factor $q_{\min}$ appears at $r=r_{\min}$. When $q_{\min}<m/n$, the corresponding mode-resonant surfaces appear at both sides of $r=r_{\min}$. When we divide the plasma region into an inner region and outer regions, the inner region $r_L<r<r_R$ is taken to cover the mode-resonant surface(s). The width of the inner region is defined by $\Delta r:=r_R-r_L$. Then the outer regions extend from $r=0$ to $r=r_L$ and from $r=r_R$ to $r=a$. The inertialess MHD equation, or the Newcomb equation,[12] is solved in the outer regions. In the inner region, on the other hand, the high-beta reduced MHD equations are solved. Then the solution in each region will be connected by the technique developed below.

In the following, the quantities are normalized by using a, B_0 that is the magnitude of the ambient magnetic field in the z direction, ρ_0 that is the mass density assumed to be constant, $v_A:=B_0/\sqrt{\mu_0\rho_0}$, where μ_0 is the vacuum permeability, and $\tau_A:=a/v_A$.

The governing equations adopted in the present paper is the large-aspect-ratio and high-beta reduced MHD equations,[20,21]

$$\frac{dU}{dt} = -\nabla_{\parallel} J + \hat{\mathbf{z}} \cdot \boldsymbol{\kappa}_0 \times \nabla_{\perp} p, \tag{1}$$

$$\frac{\partial \psi}{\partial t} + \nabla_{\parallel} \varphi = \eta J, \tag{2}$$

$$\frac{dp}{dt} = -\hat{\mathbf{z}} \cdot \nabla_{\perp} \beta \times \nabla_{\perp} \varphi. \tag{3}$$

Here, the velocity and magnetic fields are expressed by

$$\mathbf{v} = \hat{\mathbf{z}} \times \nabla \varphi, \tag{4}$$

$$\mathbf{B} = \nabla \psi \times \hat{\mathbf{z}} + \hat{\mathbf{z}}. \tag{5}$$

The vorticity in the z direction and the current in the negative z direction are expressed as

$$U = \nabla_{\perp}^2 \varphi, \tag{6}$$

$$J = \nabla_{\perp}^2 \psi, \tag{7}$$

respectively, where $\nabla_{\perp}^2$ means the Laplacian in the r-θ plane

$$\nabla_{\perp}^2 = \frac{1}{r}\frac{\partial}{\partial r}\left(r\frac{\partial}{\partial r}\right) + \frac{1}{r^2}\frac{\partial^2}{\partial \theta^2}. \tag{8}$$

The equilibrium pressure is expressed by β and the perturbed pressure by p. The equilibrium magnetic field curvature is defined by $\boldsymbol{\kappa}_0 \equiv \mathbf{b}_0 \cdot \nabla \mathbf{b}_0$, where $\mathbf{b}_0$ is the unit vector in the direction of zeroth order magnetic field. Although $\mathbf{b}_0 = \hat{\mathbf{z}}$ and thus $\boldsymbol{\kappa}_0$ becomes zero in the large-aspect ratio limit, we take into account the equilibrium poloidal magnetic field, and we set $\boldsymbol{\kappa}_0 \cdot \hat{\mathbf{r}} \equiv \kappa_{0r} = -B_{0\theta}^2 / r$. The convective and parallel derivatives are given by

$$\frac{d}{dt} \equiv \frac{\partial}{\partial t} + [\varphi, \ ], \tag{9}$$

$$\nabla_{\parallel} \equiv \varepsilon \frac{\partial}{\partial \zeta} - [\psi, \ ], \tag{10}$$

respectively, and the Poisson bracket is defined as

$$[f,g] \equiv \hat{\mathbf{z}} \cdot \nabla f \times \nabla g = \frac{1}{r}\left(\frac{\partial f}{\partial r}\frac{\partial g}{\partial \theta} - \frac{\partial f}{\partial \theta}\frac{\partial g}{\partial r}\right). \tag{11}$$

The electrical resistivity is denoted by η, which is the inverse of the Lundquist number.

Assuming that there is no equilibrium plasma flow, linearized reduced MHD equations are written as

$$\gamma \begin{pmatrix} \nabla_{\perp}^2 & 0 & 0 \\ 0 & 1 & 0 \\ 0 & 0 & 1 \end{pmatrix} \begin{pmatrix} \varphi \\ \psi \\ p \end{pmatrix} = \begin{pmatrix} 0 & -\left(in\varepsilon - \frac{im\psi_0'}{r}\right)\nabla_{\perp}^2 - \frac{imJ_0'}{r} & \frac{im\kappa_{0r}}{r} \\ -\left(in\varepsilon - \frac{im\psi_0'}{r}\right) & \eta\nabla_{\perp}^2 & 0 \\ \frac{im\beta'}{r} & 0 & 0 \end{pmatrix} \begin{pmatrix} \varphi \\ \psi \\ p \end{pmatrix}, \tag{12}$$

where the time dependence is assumed to be $e^{\gamma t}$, $\psi_0(r)$ denotes the equilibrium component of ψ, and $J_0 \equiv \nabla_{\perp}^2 \psi_0$. The prime denotes the derivative with respect to r, unless otherwise stated.

B. Outer region

In the outer region, the plasma inertia and the electrical resistivity are neglected: γ and η are set to be zero in Eq. (12). Then the Newcomb equation is obtained as follows:

$$\frac{1}{r}\frac{d}{dr}\left(r\frac{d\psi}{dr}\right) - \left[\left(\frac{m}{r}\right)^2 - \frac{J_0'}{\varepsilon r(n/m + 1/q)} - \frac{\kappa_{0r}\beta'}{\varepsilon^2 r^2 (n/m + 1/q)^2}\right]\psi = 0, \tag{13}$$

where $q = \varepsilon r / B_{\theta}$ is the safety factor with $B_{\theta} = -\psi_0'$ as the equilibrium poloidal magnetic field.

We solve Eq. (13) in $0 \le r \le r_L$ with the following boundary conditions:

$$G_{\mathrm{out,L}}(r) \propto r^m \quad \text{as} \quad r \to 0, \tag{14}$$

$$G_{\mathrm{out,L}}(r_L) = 1. \tag{15}$$

Then, ψ can be expressed as

$$\psi_{\mathrm{out,L}}(r) = \psi_L G_{\mathrm{out,L}}(r). \tag{16}$$

The factor $e^{i(m\theta + n\zeta)}$ is omitted for simplicity of the notation. The function $G_{\mathrm{out,L}}(r)$ can be considered as a Green's function, and the amplitude coefficient ψ_L will be determined later.

Similarly, we solve Eq. (13) in $r_R \le r \le 1$ with the following boundary conditions:

$$G_{\mathrm{out,R}}(r_R) = 1, \tag{17}$$

$$G_{\mathrm{out,R}}(1)=0. \tag{18}$$

Then, ψ can be expressed as

$$\psi_{\mathrm{out,R}}(r)=\psi_{\mathrm{R}}G_{\mathrm{out,R}}(r). \tag{19}$$

Finally, we would like to mention that our matching technique can also be applied for free boundary modes by changing the boundary condition $G_{\mathrm{out,R}}(1)=0$ to an appropriate one.

C. Inner region

In the inner region, we solve Eq. (12). This equation is not the so-called "inner-layer equation" where the radial coordinate and the frequency are expanded by using a small parameter related to resistivity.

In order to obtain Green's functions in the inner region, we solve Eq. (12) as a boundary-value problem by giving a guess value γ. Let us denote $\mathbf{G}=^{\mathrm{t}}(\varphi,\psi,p)$. Since the pressure equation has no radial derivative in Eq. (12), the order of radial derivative of Eq. (12) is 4 in total, and thus four independent solutions can be obtained for the following four boundary conditions:

$$\mathbf{G}_{\mathrm{in,L,1}}(r_{\mathrm{L}})=\begin{pmatrix}*\\1\\-\end{pmatrix},\quad \mathbf{G}_{\mathrm{in,L,1}}(r_{\mathrm{R}})=\begin{pmatrix}*\\0\\-\end{pmatrix}, \tag{20}$$

$$\mathbf{G}_{\mathrm{in,L,2}}(r_{\mathrm{L}})=\begin{pmatrix}1\\0\\-\end{pmatrix},\quad \mathbf{G}_{\mathrm{in,L,2}}(r_{\mathrm{R}})=\begin{pmatrix}*\\0\\-\end{pmatrix}, \tag{21}$$

$$\mathbf{G}_{\mathrm{in,R,1}}(r_{\mathrm{L}})=\begin{pmatrix}*\\0\\-\end{pmatrix},\quad \mathbf{G}_{\mathrm{in,R,1}}(r_{\mathrm{R}})=\begin{pmatrix}*\\1\\-\end{pmatrix}, \tag{22}$$

$$\mathbf{G}_{\mathrm{in,R,2}}(r_{\mathrm{L}})=\begin{pmatrix}*\\0\\-\end{pmatrix},\quad \mathbf{G}_{\mathrm{in,R,2}}(r_{\mathrm{R}})=\begin{pmatrix}1\\0\\-\end{pmatrix}, \tag{23}$$

where the meaning of the asterisks will be explained in the following three paragraphs, and − in each third row means that no boundary condition is required for p since there is no radial derivative of p. When we include a heat diffusivity term, $\chi\nabla_{\perp}^2 p$, on the right-hand side of the pressure equation, we need a boundary condition also for p. This is described in Appendix A. The ψ component of $\mathbf{G}_{\mathrm{in,L,1}}(r)$, denoted by $G_{\mathrm{in,L,1}}(r)$, becomes unity at $r=r_{\mathrm{L}}$ and becomes zero at the other side $r=r_{\mathrm{R}}$. On the other hand, $G_{\mathrm{in,R,1}}(r)$ becomes zero at $r=r_{\mathrm{L}}$ and becomes unity at the other side $r=r_{\mathrm{R}}$. As for $\mathbf{G}_{\mathrm{in,L,2}}(r)$ and $\mathbf{G}_{\mathrm{in,R,2}}(r)$, the φ components become unity at $r=r_{\mathrm{L}}$ and r_{R}, respectively, and the ψ components becomes zero at both sides. This choice of the Green's functions gives us four independent solutions suitable for the inner region or the resistive MHD region.

The asterisks that appeared in the boundary conditions (20)–(23) denote that a boundary condition of the third kind is imposed for φ,

$$\frac{\mathrm{d}\varphi}{\mathrm{d}r}=\left(\frac{\psi'}{\psi}+\frac{\mathrm{i}m}{r}\frac{\psi_0''-\psi_0'/r}{\mathrm{i}n\varepsilon-\mathrm{i}m\psi_0'/r}\right)\varphi. \tag{24}$$

This is obtained from the linearized ideal Ohm's law,

$$E_{\parallel}=-\gamma\psi-\left(\mathrm{i}n\varepsilon-\frac{\mathrm{i}m\psi_0'}{r}\right)\varphi=0 \tag{25}$$

and its radial derivative $E_{\parallel}'=0$, where $E_{\parallel}$ denotes the parallel electric field. Since the solution in the inner region must match onto the solution in the outer region where the ideal MHD equation is satisfied, $E_{\parallel}$ must approach zero smoothly as approaching the boundaries of the inner region. Thus, we require $E_{\parallel}$ and $E_{\parallel}'$ approach zero smoothly. Equation (24) was derived by using these conditions. However, the inverse is not necessarily true; $E_{\parallel}=0$ and $E_{\parallel}'=0$ lead to Eq. (24), but Eq. (24) does not necessarily lead to $E_{\parallel}=0$ and $E_{\parallel}'=0$. If we assume that Eq. (24) is given, $E_{\parallel}'$ can be expressed as

$$\begin{aligned}E_{\parallel}'&=-\gamma\psi'-\left(\mathrm{i}n\varepsilon-\frac{\mathrm{i}m\psi_0'}{r}\right)\varphi'-\left(\mathrm{i}n\varepsilon-\frac{\mathrm{i}m\psi_0'}{r}\right)'\varphi\\&=E_{\parallel}\frac{\psi'}{\psi}.\end{aligned} \tag{26}$$

From the first to the second line, Eq. (24) was used to eliminate φ'. Therefore, when Eq. (24) is imposed, $E_{\parallel}'$ approaches zero if $E_{\parallel}$ approaches zero. Therefore, $\mathbf{G}_{\mathrm{in,L,1}}$ and $\mathbf{G}_{\mathrm{in,R,1}}$ are chosen so that $E_{\parallel}$ and $E_{\parallel}'$ approach zero smoothly at both sides $r=r_{\mathrm{L}}$ and r_{R}, and the ψ components of $\mathbf{G}_{\mathrm{in,L,1}}$ ($\mathbf{G}_{\mathrm{in,R,1}}$) are unity (zero) at $r=r_{\mathrm{L}}$ and zero (unity) at $r=r_{\mathrm{R}}$.

Let us examine the consistency of our boundary condition (24) with the asymptotic behavior of $E_{\parallel}$ in the conventional asymptotic matching theory. The inner-layer equation can be written as

$$\Gamma\frac{\mathrm{d}^2\varphi}{\mathrm{d}X^2}=-\mathrm{i}X\frac{\mathrm{d}^2\psi}{\mathrm{d}X^2}+\mathrm{i}D_{\mathrm{S}}P, \tag{27}$$

$$\Gamma\psi=-\mathrm{i}X\varphi+\frac{\mathrm{d}^2\psi}{\mathrm{d}X^2}, \tag{28}$$

$$\Gamma P=\mathrm{i}\varphi, \tag{29}$$

where $\Gamma:=\gamma/\{\eta[m\varepsilon(1/q)']^2\}^{1/3}$ and $X:=(r-r_{\mathrm{s}})/\{\eta/[m\varepsilon(1/q)']\}^{1/3}$ are the stretched growth rate and radial coordinate, respectively, $P:=p(r/m\beta')\{\eta[m\varepsilon(1/q)']^2\}^{1/3}$ is the scaled perturbed pressure, and $D_{\mathrm{S}}:=-\beta'(q/q')^2/r$ is the Suydam index.[23] All the equilibrium quantities are evaluated at the mode-resonant surface $r=r_{\mathrm{s}}$. Assuming the inverse-power series in $|X|$ at large $|X|$, we obtain the following big and small solutions in the leading order as

$$\varphi=\pm\mathrm{i}\Gamma\psi_{\infty\mathrm{L,R}}(|X|^{-1/2-\mu}+a_{\mathrm{L,R}}|X|^{-1/2+\mu}), \tag{30}$$

$$\psi=\psi_{\infty\mathrm{L,R}}(|X|^{1/2-\mu}+a_{\mathrm{L,R}}|X|^{1/2+\mu}), \tag{31}$$

$$P=\mp\psi_{\infty\mathrm{L,R}}(|X|^{-1/2-\mu}+a_{\mathrm{L,R}}|X|^{-1/2+\mu}), \tag{32}$$

where $\psi_{\infty\mathrm{L}}$ and $\psi_{\infty\mathrm{R}}$ are the arbitrary amplitude coefficients at $X\to-\infty$ and $X\to+\infty$, respectively, and a_{L} and a_{R} are the corresponding matching data. In the vorticity equation, we

take the plus sign on the right-hand side for $X \to -\infty$ and the minus sign for $X \to \infty$. In the pressure equation, we take the minus sign on the right-hand side for $X \to -\infty$ and the plus sign for $X \to \infty$. By using these asymptotic forms, we obtain

$$\frac{1}{\varphi}\frac{d\varphi}{dX} = \frac{-1}{|X|(1+a_{L,R}|X|)}, \tag{33}$$

$$\frac{1}{\psi}\frac{d\psi}{dX} = \frac{\pm a_{L,R}}{(1+a_{L,R}|X|)}. \tag{34}$$

On the other hand, let us derive an asymptotic form of our boundary condition (24). In the region near the mode-resonant surface, Eq. (24) can be approximated as

$$\varphi' = \left(\frac{\psi'}{\psi} - \frac{1}{x}\right)\varphi. \tag{35}$$

By introducing the stretched radial coordinate X, this can be rewritten as

$$\frac{d\varphi}{dX} = \left(\frac{1}{\psi}\frac{d\psi}{dX} - \frac{1}{X}\right)\varphi. \tag{36}$$

By substituting Eqs. (33) and (34) into this equation, we can confirm that the asymptotic form of our boundary condition is satisfied by Eqs. (33) and (34). Therefore, the boundary condition (24) is consistent with the conventional asymptotic matching theory in the limit of infinitely thin inner layer.

There is no need to refer to $\mathbf{G}_{in,L,2}$ and $\mathbf{G}_{in,R,2}$ actually since only two of the four Green's functions can be matched onto the solutions in the ideal MHD region and since the boundary conditions for $\mathbf{G}_{in,L,1}$ and $\mathbf{G}_{in,R,1}$ are chosen so that they can be matched onto the solutions in the ideal MHD regions. Thus, redefining $\mathbf{G}_{in,L,1}$ and $\mathbf{G}_{in,R,1}$ as $\mathbf{G}_{in,L}$ and $\mathbf{G}_{in,R}$, respectively, then the solution in the inner region can be expressed as

$$\begin{pmatrix} \varphi \\ \psi \\ p \end{pmatrix} = \psi_L \mathbf{G}_{in,L}(r;\gamma) + \psi_R \mathbf{G}_{in,R}(r;\gamma). \tag{37}$$

In Eq. (24), ψ'/ψ appears on the right-hand side. It is evaluated as $G'_{out,L}/G_{out,L}$ at $r=r_L$ and $G'_{out,R}/G_{out,R}$ at $r=r_R$. When the matching is completed and the eigenfunctions are obtained, these replacement is valid.

D. Dispersion relation

The ψ component of Eq. (37),

$$\psi(r) = \psi_L G_{in,L}(r;\gamma) + \psi_R G_{in,R}(r;\gamma), \tag{38}$$

has been already chosen to be continuous across the boundaries $r=r_L$ and r_R, where $G_{in,L}$ and $G_{in,R}$ denote the ψ components of $\mathbf{G}_{in,L}$ and $\mathbf{G}_{in,R}$, respectively. We further impose continuity of $d\psi/dr$ across the boundaries $r=r_L$ and r_R, then we obtain the following dispersion relation:

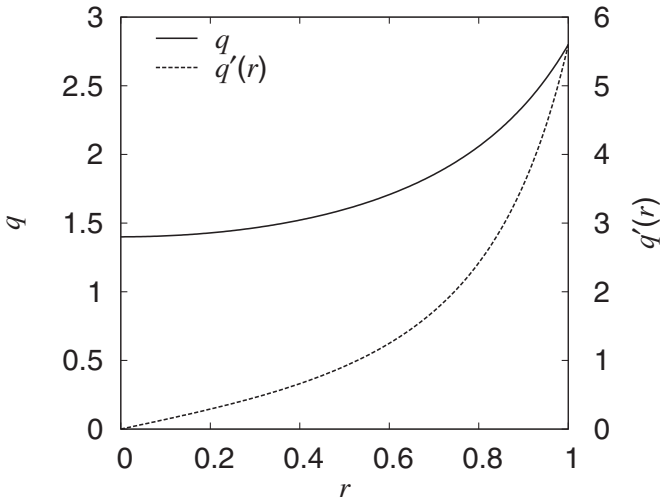

FIG. 1. Equilibrium q and $q'(r)$ profiles for the calculation of $m/n=3/2$ and 2/1 tearing modes in normal magnetic shear plasmas.

$$\begin{pmatrix} G'_{in,L}(r_L;\gamma) - G'_{out,L}(r_L) & G'_{in,R}(r_L;\gamma) \\ G'_{in,L}(r_R;\gamma) & G'_{in,R}(r_R;\gamma) - G'_{out,R}(r_R) \end{pmatrix} \times \begin{pmatrix} \psi_L \\ \psi_R \end{pmatrix} = 0. \tag{39}$$

If we denote the matrix on the left-hand side as $\mathsf{A}(\gamma)$, the true eigenvalue γ can be obtained by $\det \mathsf{A}(\gamma)=0$. In numerical calculations, the Newton–Raphson method was used to obtain the true eigenvalue starting from a guess value γ.

E. Applications

1. m/n=3/2 and 2/1 tearing modes in normal magnetic shear plasmas

The first application is to the $m/n=3/2$ and 2/1 tearing modes in normal magnetic shear plasmas. The conventional asymptotic matching theory has been developed for these modes, and the resistivity dependence of the growth rate is known to be $\eta^{3/5}$. It will be shown below that our numerical matching technique reproduces this dependence, especially when the resistivity is small enough or when the conventional asymptotic matching method gives us a good approximation.

The equilibrium current density profile is set to be $j_t(r) = j_{t0}(1-r^2)$ with $q_a=2.8$. Then the radial positions of the mode-resonant surfaces are $r=0.365$ and 0.774 for $m/n=3/2$ and 2/1, respectively. The equilibrium q and q' profiles are shown in Fig. 1. The equilibrium pressure is assumed to be zero. The tearing mode stability parameters are $\Delta'=6.74$ and 13.9 for $m/n=3/2$ and 2/1, respectively.

First of all, the growth rate γ of the tearing mode, calculated by our numerical matching technique, is plotted as a function of plasma resistivity η in Fig. 2. By the conventional asymptotic matching, the growth rate in the physical dimension is obtained as[24]

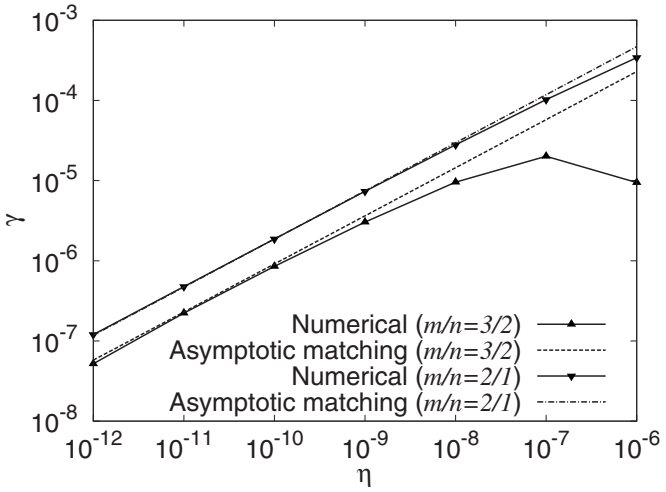

FIG. 2. Eigenvalues γ of $m/n=3/2$ and 2/1 tearing modes in normal magnetic shear plasmas are plotted as a function of the plasma resistivity η. At sufficiently small η, our results agree well with the results by the conventional asymptotic matching theory. At relatively large η, the conventional asymptotic matching theory cannot be applied. Even for this range of η, our numerical matching technique is applicable, and we observe the deviation from the $\gamma \propto \eta^{3/5}$ dependence.

$$\gamma_{\rm phys} = \frac{0.55}{\tau_R^{3/5}\tau_A^{2/5}}\left(\frac{a}{R}\frac{naq'}{q}\right)^{2/5}(a\Delta')^{4/5}, \tag{40}$$

where $\tau_R := \mu_0 a^2/\eta$ is the resistive time, $\tau_A := v_A/a$ is the Alfvén time, a and R are the minor and major radii, respectively, n is the toroidal mode number, and q and q' are the safety factor and its radial derivative, respectively. By using the normalization in our paper and substituting the parameters used in the numerical calculation, the growth rates can be expressed as $\gamma=0.913\eta^{3/5}$ and $1.87\eta^{3/5}$ for $m/n=3/2$ and 2/1, respectively. These are plotted together in Fig. 2. We observe good agreement between them at sufficiently small η. We also observe that γ deviates from the $\eta^{3/5}$ dependence at relatively large η, where the assumption for the conventional asymptotic matching theory breaks down. Our numerical matching technique is also applicable to this range of η. In calculating this growth rate, the inner region was chosen such that it is centered at the mode-resonant surface. For $\eta=10^{-12}$, the inner-region width was 0.16 with 1302 accumulated grids for $m/n=3/2$ and 0.08 with 1024 uniform grids for $m/n=2/1$, respectively. For larger η, wider Δr is required to obtain sufficient accuracy; however, the number of grids in the unit width of the inner region can be reduced. For example, 80 grids in $\Delta r=0.1$ were sufficient to obtain good accuracy for $\eta=10^{-8}$.

Figure 3 shows the eigenvalue γ as a function of Δr, normalized by $\gamma_{\rm global}$, which is the growth rate obtained by a calculation where Eq. (12) was solved as an eigenvalue problem in the whole plasma domain without the numerical matching. Figures 3(a) and 3(b) are for $m/n=3/2$, and Figs. 3(c) and 3(d) are for $m/n=2/1$. At $\Delta r=1$, $\gamma_{\rm global}$ is just plotted. The horizontal axis label is Δr for Figs. 3(a) and 3(c) and $\Delta r/x_r$ for Figs. 3(b) and 3(d), where x_r is the resistive-layer width defined by $x_r := |r/nB_\theta q'|^{1/3}\eta^{1/3}$ evaluated at the rational surface. The resistive-layer widths in this case are

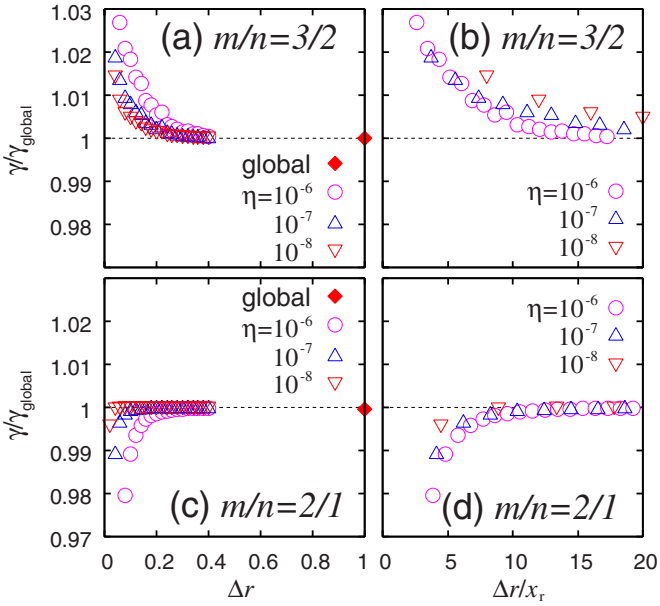

FIG. 3. (Color online) Eigenvalues of $m/n=3/2$ and 2/1 tearing modes in normal magnetic shear plasmas, normalized by eigenvalues obtained without numerical matching technique. The horizontal axis labels are (a),(c) Δr and (b),(d) $\Delta r/x_r$. The error of $\gamma/\gamma_{\rm global}$ is less than several percent even if the inner-region width is only five times the resistive-layer width.

$x_r=2.32\eta^{1/3}$ and $2.08\eta^{1/3}$ for $m/n=3/2$ and 2/1, respectively. When the width of the inner region Δr is changed, the radial grid size was kept unchanged. We find that γ is accurately obtained by this numerical matching technique. The error of $\gamma/\gamma_{\rm global}$ is several percent or less when the inner-region width is taken as five times the resistive-layer width. This accuracy would be sufficient in actual applications. The behavior of $\gamma/\gamma_{\rm global}$ as a function of $\Delta r/x_r$ is similar for a range of η in both cases of $m/n=3/2$ and 2/1. The data points seem to be on a curve especially for $m/n=2/1$. Therefore, the convergence property seems to be uniform. A smaller Δr can be used when the magnetic shear is larger.

Figure 4 shows the eigenfunctions for $\eta=10^{-8}$. Figures 4(a)–4(c) are Im φ, Re ψ, and Re $E_\parallel$ for $m/n=3/2$, respectively, and Figs. 4(d)–4(f) are Im φ, Re ψ, and Re $E_\parallel$ for $m/n=2/1$, respectively. The equation for the perturbed pressure p decouples from the others, and thus no figure is shown for p. The parallel electric field $E_\parallel$ was calculated after the eigenfunctions φ and ψ were obtained. The eigenfunctions in the inner region obtained by the numerical matching are overlaid on the eigenfunctions by the global calculation (without the matching). We find that the eigenfunctions agree well with those of the global solution.

As the plasma resistivity is decreased, the mode structure becomes more localized around the mode-resonant surface. Thus, we can use smaller Δr for obtaining sufficiently accurate eigenvalues and eigenfunctions. Thus, the computational cost is reduced significantly. Therefore, this matching technique is more advantageous especially for high-temperature plasmas.

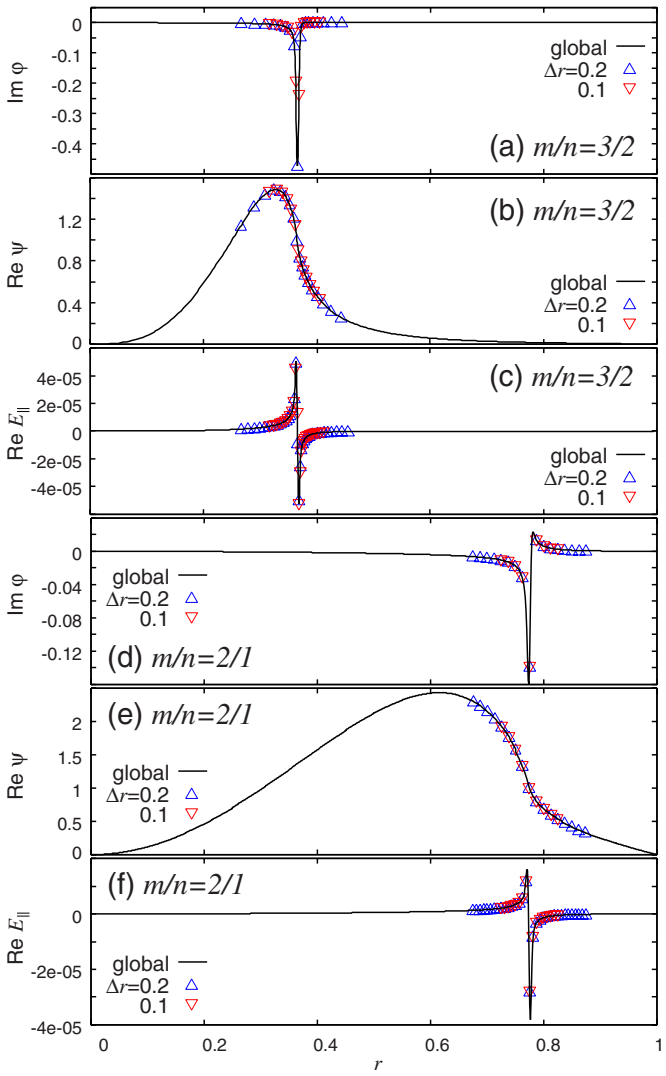

FIG. 4. (Color online) Eigenfunctions of [(a)–(c)] $m/n=3/2$ and [(d)–(f)] $m/n=2/1$ tearing modes in normal magnetic shear plasmas with $\eta=10^{-8}$. (a) and (d) are imaginary parts of φ, (b) and (e) are real parts of ψ, (c) and (f) are real parts of $E_\parallel$. We find good agreement between the eigenfunctions with and without our numerical matching technique.

2. m/n=1/1 internal kink modes in normal magnetic shear plasmas

The second application is to the $m/n=1/1$ internal kink mode in normal magnetic shear plasmas. The conventional asymptotic matching theory has also been developed for this mode, and the resistivity dependence of the growth rate is known to be $\eta^{1/3}$. It will be shown below that this dependence is also reproduced by using our matching method, like $m/n=3/2$ and $2/1$ tearing modes, especially when the resistivity is small enough or when the conventional asymptotic matching method gives us a good approximation.

The equilibrium current density profile is set to be again $j_t(r)=j_{t0}(1-r^2)$ with $q_a=3.95$. Then the mode-resonant surface for $m/n=1/1$ mode appears at $r=0.05$. The equilibrium q and q' profiles are shown in Fig. 5. The equilibrium pressure is assumed to be zero. In this case, r_L was set to be zero, and the boundary condition $\varphi(0)=\psi(0)=0$ was used. The present matching method works well, of course, even for this one-sided situation.

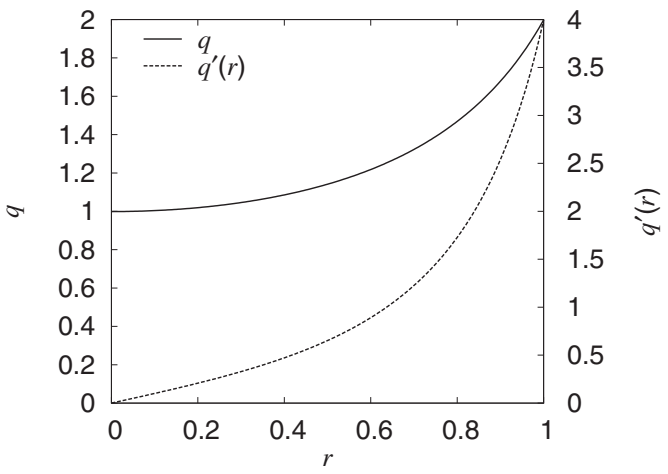

FIG. 5. Equilibrium q and $q'(r)$ profiles for the calculation of $m/n=1/1$ internal kink modes in normal magnetic shear plasmas.

Figure 6 shows the growth rate γ of the internal kink mode, calculated by our numerical matching technique as a function of plasma resistivity η. By the conventional asymptotic matching, the growth rate in the physical dimension is obtained as[24]

$$\gamma_{\rm phys}=\frac{(q'B_\theta/\sqrt{\mu_0\rho})^{2/3}}{(\mu_0 r^2/\eta)^{1/3}}. \tag{41}$$

By using the normalization in our paper and substituting the parameters used in the numerical calculation, the growth rate can be expressed as $\gamma=0.029\eta^{1/3}$. This is plotted together in Fig. 6. We observe good agreement between them at sufficiently small η. We also observe that γ deviates from the $\eta^{1/3}$ dependence at relatively large η. This deviation is because the assumption for the conventional asymptotic matching theory breaks down at large η. Also γ seems to be af-

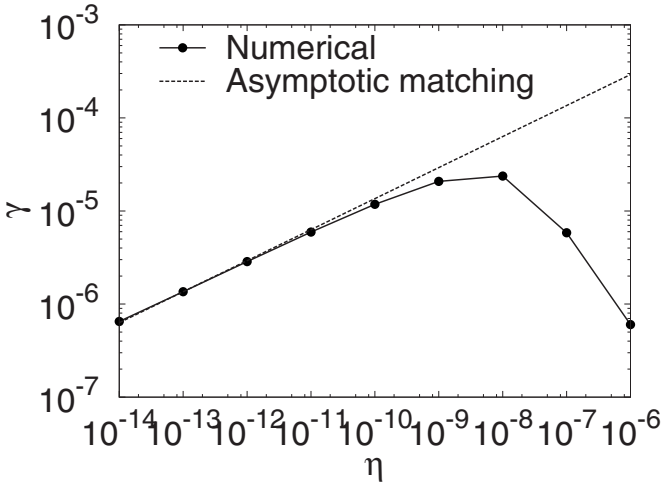

FIG. 6. Eigenvalues γ of $m/n=1/1$ internal kink modes in normal magnetic shear plasmas are plotted as a function of the plasma resistivity η. At sufficiently small η, our results agree well with the results by the conventional asymptotic matching theory. At relatively large η, the conventional asymptotic matching theory cannot be applied. Even for this range of η, our numerical matching technique is applicable, and we observe the deviation from the $\gamma\propto\eta^{1/3}$ dependence.

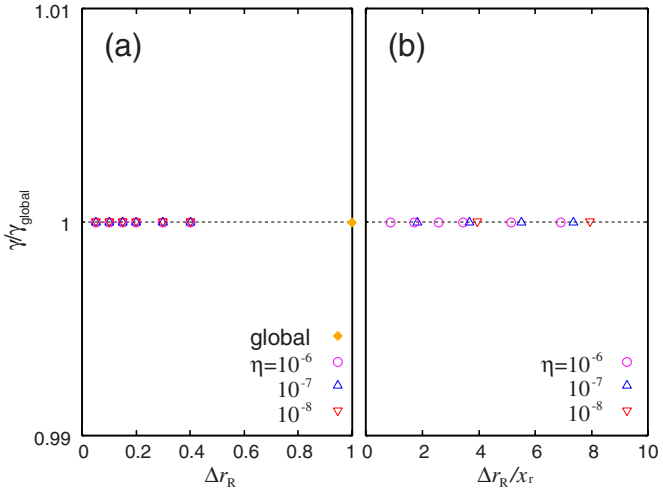

FIG. 7. (Color online) Eigenvalues of $m/n=1/1$ internal kink modes in normal magnetic shear plasmas, normalized by eigenvalues obtained without numerical matching technique. The horizontal axis labels are (a) Δr_R and (b) $\Delta r_R/x_r$. The error of γ/γ_{global} is much less than 1% even if Δr_R is only one resistive-layer width.

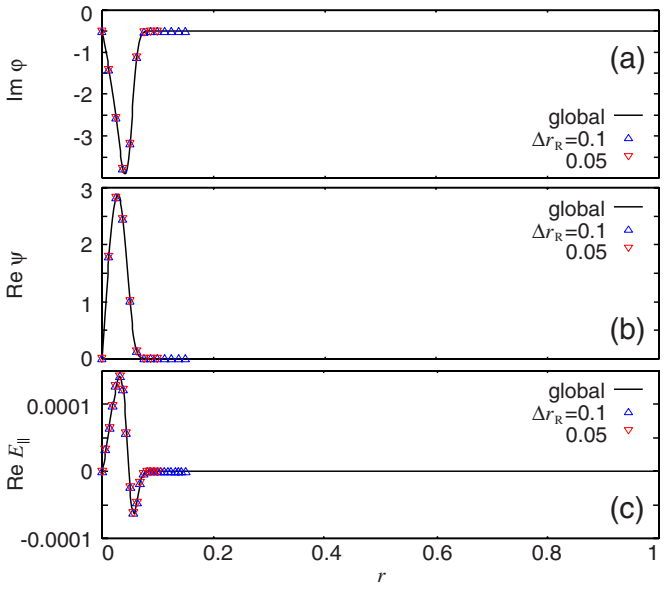

FIG. 8. (Color online) Eigenfunctions of $m/n=1/1$ internal kink modes in normal magnetic shear plasmas with $\eta=10^{-8}$. (a) Imaginary part of φ, (b) real part of ψ, and (c) real part of $E_{\parallel}$. We find good agreement between the eigenfunctions with and without our numerical matching technique.

fected by the boundary condition at the magnetic axis since the mode-resonant surface for $q=1$ is close to the magnetic axis, especially when η is large. Our numerical matching technique is also applicable to this range of parameters. The width of the inner region $\Delta r_R=0.01$ was used for $\eta=10^{-14}$, where Δr_R denotes the distance from the mode-resonance $r_s=0.05$ to the boundary r_R. The number of grids was 500 in the inner region of the total width $\Delta r=0.06$. For larger η, wider Δr_R is required to obtain sufficient accuracy; however, the number of grids in the unit width of the inner region can be reduced. For example, 80 grids in the total width $\Delta r=0.1$ were sufficient to obtain good accuracy for $\eta=10^{-8}$.

Figure 7 shows the normalized eigenvalues. The horizontal axis label is Δr_R for (a) and $\Delta r_R/x_r$ for (b), where the resistive-layer width is $x_r=5.85\eta^{1/3}$ in this case. Even if Δr_R is one or two times the resistive-layer width, the error of γ/γ_{global} is much less than 1%. Since the error is too small, we cannot observe clear convergence property in this case. Figure 8 shows the eigenfunctions for $\eta=10^{-8}$. The eigenfunctions in the inner region obtained by the numerical matching are overlaid on the eigenfunctions by the global calculation (without the matching). The eigenfunctions obtained by using our numerical matching technique agree well with those of global calculation. As in the tearing mode cases presented above, a better convergence is obtained even for smaller Δr_R when the magnetic shear is larger.

Stability of internal kink mode is an essential factor in studying sawtooth oscillations.[4,25] Two-fluid effects seem to be required at least to explain characteristics of sawtooth. One of the advantages to use the inner layer, both in the conventional asymptotic matching theory and in our numerical matching technique, is that the inner-layer equation can be extended to include such effects relatively easily. Extension of the present technique and its application to the sawtooth problem may be a future issue.

Finally, we would like to mention that the numerical matching for large r_s, say $r_s=0.5$, with $r_L\neq 0$ does not give good accuracy, especially when the resistivity is not sufficiently small. Among applications we have done, this internal kink mode with large r_s and large η was only the special case. This situation is discussed in Appendix B.

3. m/n=2/1 resistive interchange modes in normal magnetic shear plasmas

The third application is to the $m/n=2/1$ resistive interchange mode in normal magnetic shear plasmas. The conventional asymptotic matching theory predicts that the resistivity dependence of the growth rate is $\eta^{1/3}$. It will be shown below that our numerical matching technique reproduces this dependence, especially when the resistivity is small enough or when the conventional asymptotic matching method gives us a good approximation.

The equilibrium safety factor profile is set to be $q(r)=q_a/(2-r^2)+\beta_q(r-r_s)e^{-(r-r_s)^2/L_q^2}$ with $q_a=3.5$, $\beta_q=-0.3$, and $L_q=0.1$. When $\beta_q=0$, this q profile corresponds to the toroidal current density profile $j_t(r)=j_{t0}(1-r^2)$ used in the previous subsections. In order to stabilize the $m/n=2/1$ tearing mode, the modulation term proportional to β_q is introduced, which makes the q profile flatter around $r=r_s$ when $\beta_q<0$. The mode-resonant surface for $m/n=2/1$ mode appears at $r=0.5$. The equilibrium q and q' profiles are shown in Fig. 9(a). In addition, finite equilibrium plasma pressure $\beta(r)$ is introduced in this subsection. The profile is set to be $\beta(r)=\beta_0(1-r^2)$ with $\beta_0=0.01$. This is plotted in Fig. 9(b), together with the Suydam index D_S. This equilibrium is Suydam stable at $r=r_s$. The tearing mode parameter is $\Delta'=-22.3$ for $\beta_0=0$ and $\Delta'=-3.23$ for $\beta_0=0.01$.

Figure 10 shows the growth rate γ of the resistive interchange mode, calculated by our numerical matching technique, as a function of plasma resistivity η. By the conventional asymptotic matching, the growth rate is known to be

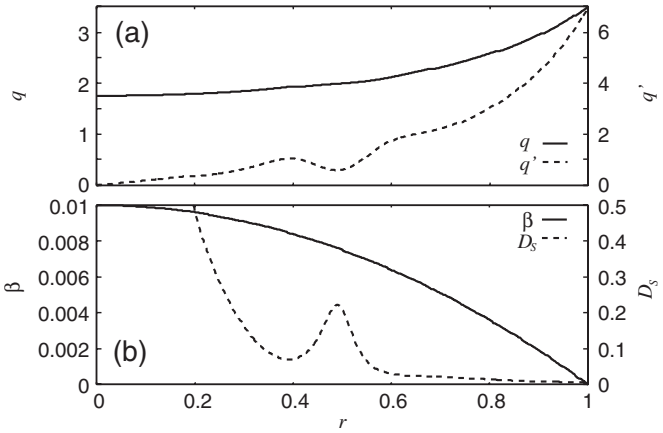

FIG. 9. Equilibrium q, q', β, and D_S profiles for the calculation of $m/n=2/1$ resistive interchange modes in normal magnetic shear plasmas. (a) q and q', (b) β and D_S.

proportional to $\eta^{1/3}$. We observe good agreement between our numerical results with the analytic scaling at sufficiently small η. We also observe that γ deviates from the $\eta^{1/3}$ dependence at relatively large η as in the tearing and internal kink modes, where the assumption for the conventional asymptotic matching theory breaks down. Our numerical matching technique is also applicable to this range of η. In calculating this growth rate, the inner region was chosen such that it is centered at the mode-resonant surface. The width of the inner region Δr was 0.01 for $\eta=10^{-12}$, and 512 uniform grids were used in the inner region. On the other hand, 80 grids in $\Delta r=0.1$ were sufficient to obtain good accuracy for $\eta=10^{-8}$.

Figure 11 shows the eigenvalue γ normalized by γ_{global}. The horizontal axis label is Δr for (a) and $\Delta r/x_r$ for (b), where the resistive-layer width $x_r=3.19\eta^{1/3}$ in this case. When the width of the inner region Δr is changed, the number of grids were kept constant as 80 in the interval of 0.1 in the r direction. Even if the inner-region width is several times the resistive-layer width, the error of $\gamma/\gamma_{\text{global}}$ is well within several percent. This accuracy would be sufficient for actual applications. The normalized growth rate $\gamma/\gamma_{\text{global}}$ is on a curve as a function of $\Delta r/x_r$ for a range of η. Therefore, the convergence property seems to be uniform.

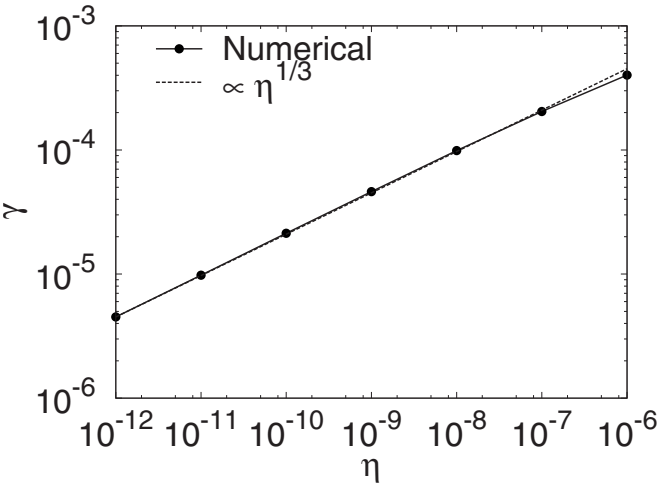

FIG. 10. Eigenvalues γ of $m/n=2/1$ resistive interchange modes in normal magnetic shear plasmas are plotted as a function of plasma resistivity η. At sufficiently small η, the conventional asymptotic matching theory predicts $\gamma\propto\eta^{1/3}$, and our results agree well with it. At relatively large η, the conventional asymptotic matching theory cannot be applied. Even for this range of η, our numerical matching technique is applicable, and we observe the deviation from the $\gamma\propto\eta^{1/3}$ dependence.

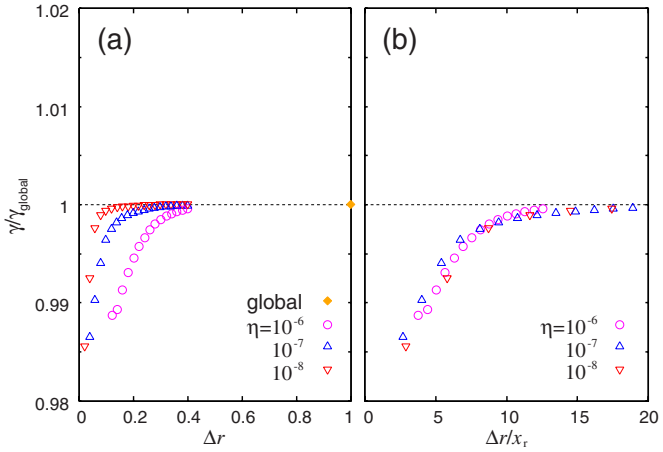

FIG. 11. (Color online) Eigenvalues of $m/n=2/1$ resistive interchange modes in normal magnetic shear plasmas, normalized by eigenvalues obtained without numerical matching technique. The horizontal axis labels are (a) Δr and (b) $\Delta r/x_r$. The error of $\gamma/\gamma_{\text{global}}$ is well within several percent even if the inner-region width is only several times the resistive-layer width.

Figure 12 shows the eigenfunctions for $\eta=10^{-8}$. The parallel electric field $E_\parallel$ was calculated after the eigenfunctions φ and ψ were obtained. The eigenfunctions in the inner region obtained by the numerical matching are overlaid on the eigenfunctions by the global calculation (without the matching). We find that the eigenfunctions agree well with those of the global solution.

4. m/n=2/1 double tearing modes in reversed magnetic shear plasmas

The final and important application is to the $m/n=2/1$ double tearing mode in reversed magnetic shear plasmas. As explained in Sec. I, the conventional asymptotic matching theory fails when the minimum safety factor is a rational number since that mode-resonant surface becomes an irregular singular point. In addition to this rather mathematical reason, another importance of the application to the double tearing mode is that the stability calculation of the mode itself is an important issue for clarifying the behavior of reversed magnetic shear plasmas when the minimum safety factor tries to go through rational numbers during current ramp up; a disruption often occurs in experiments even if the beta is low.

We assume the equilibrium safety factor q profile as

$$q(r)=q_{\min}\left[(\alpha-1)\left(\frac{r}{r_{\min}}\right)^4-2(\alpha-1)\left(\frac{r}{r_{\min}}\right)^2+\alpha\right] \quad (42)$$

with $r_{\min}=0.6$ and $\alpha=3$. The equilibrium q and q' profiles with $q_{\min}=2$ are shown in Fig. 13. The equilibrium pressure is assumed to be zero.

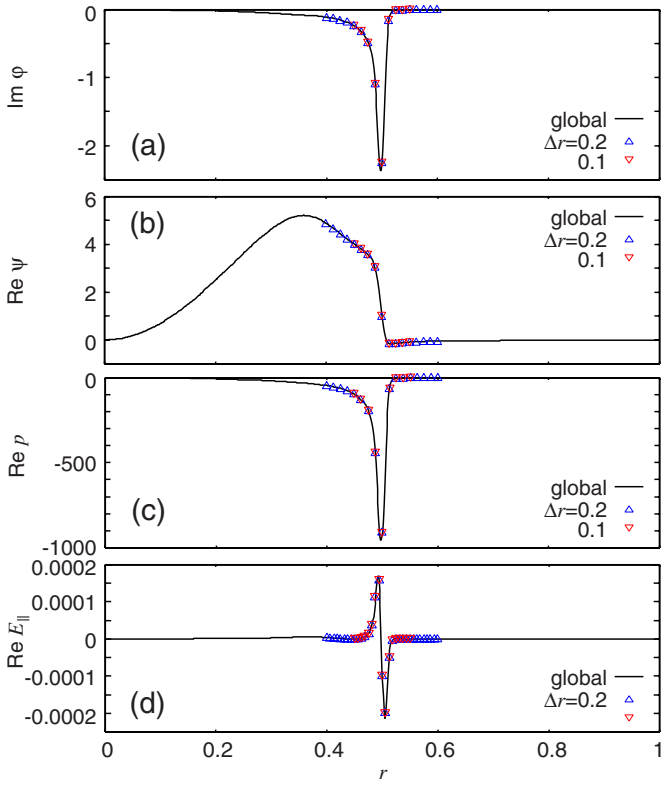

FIG. 12. (Color online) Eigenfunctions of $m/n=2/1$ resistive interchange modes in normal magnetic shear plasmas with $\eta=10^{-8}$. (a) Imaginary part of φ, (b) real part of ψ, (c) real part of p, and (d) real part of $E_{\parallel}$. We find good agreement between the eigenfunctions with and without our numerical matching technique.

Figure 14 shows the growth rate γ as a function of $q_{\min}$. These data were obtained without the numerical matching technique as a reference. The growth rate γ is larger for larger plasma resistivity η when $q_{\min}$ is relatively small or when the distance between two mode-resonant surfaces Δr_s is large. On the other hand, when $q_{\min}$ becomes close to 2, γ decreases rapidly for larger η, and thus γ becomes larger for smaller η. This is related to the distance between two resonant surfaces and the resistive-layer width. When η is small enough, the corresponding resistive layer is thinner than Δr_s. If Δr_s is small, the mode structure becomes double tearing type. When Δr_s becomes large enough, on the other hand, the mode structure becomes like two single tearing modes.[26] When Δr_s is small and the resistivity is large enough, two resistive layers at each mode-resonant surface overlap each other. The resistivity dependence of the growth rate depends on the relationship between Δr_s and resistive-layer width.

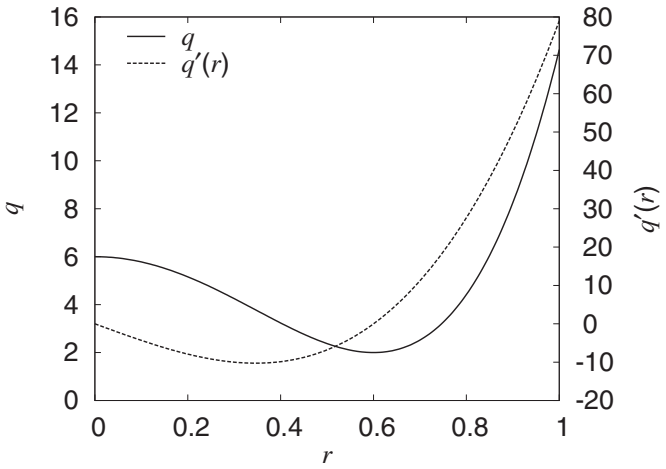

FIG. 13. Equilibrium q and $q'(r)$ profiles for the calculation of $m/n=2/1$ double tearing modes in reversed magnetic shear plasmas. Plotted is for $q_{\min}=2$.

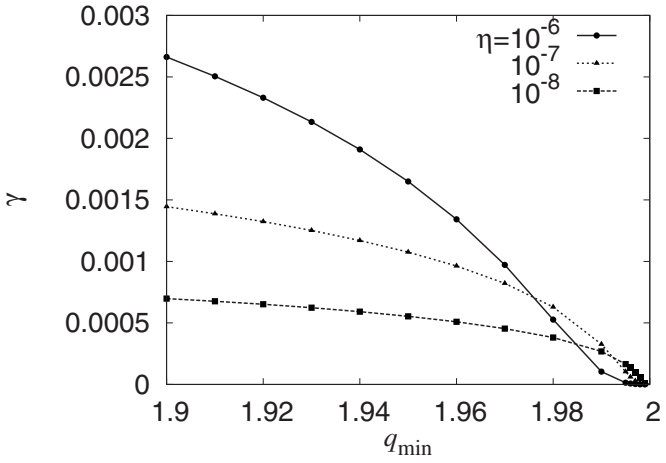

FIG. 14. Eigenvalues γ of $m/n=2/1$ double tearing modes in reversed magnetic shear plasmas for plasma resistivities of $\eta=10^{-6}$, 10^{-7}, and 10^{-8}.

Figure 15 shows the resistivity η dependence of the growth rate γ for $q_{\min}=1.99$ as an example. These data were obtained without the numerical matching technique again as in Fig. 14. The growth rate γ decreases as η is increased around $\eta\sim 10^{-6}$. On the other hand, γ is proportional to $\eta^{1/3}$ for small η. The dependence of the growth rate γ on the plasma resistivity η for $m/n=3/1$ double tearing modes was obtained numerically in Ref. 26. It was shown that the exponent x, if we assume that $\gamma\propto\eta^x$, takes a value from 1/3 to

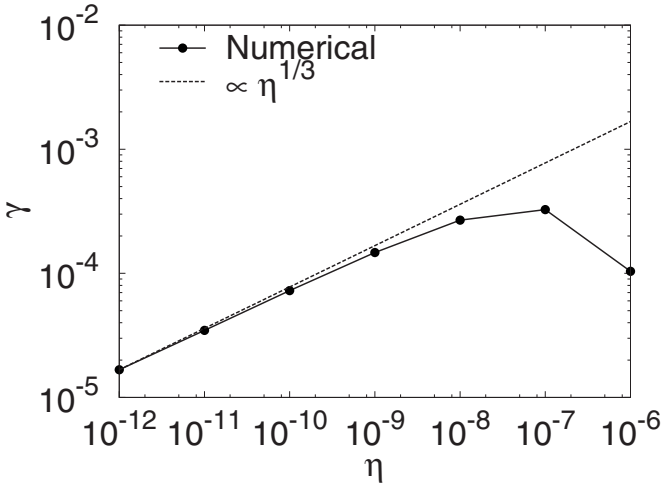

FIG. 15. Eigenvalues γ of $m/n=2/1$ double tearing modes in reversed magnetic shear plasmas with $q_{\min}=1.99$ are plotted as a function of the plasma resistivity η. Although this figure was plotted without the numerical matching technique as a reference, we stress that the numerical results by our numerical matching technique agree well with this magnitude of the growth rate as well as the resistivity dependence.

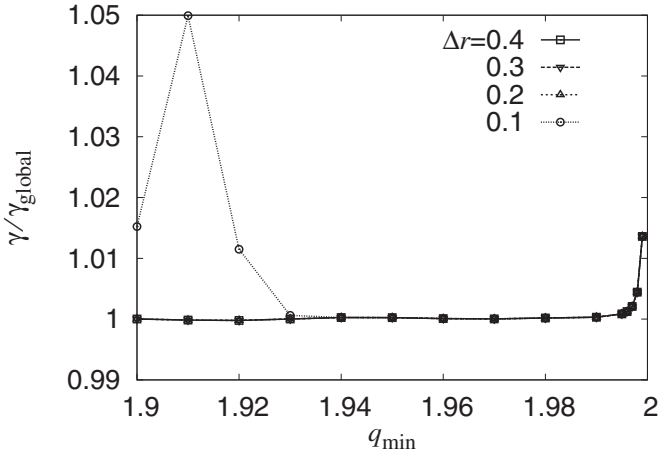

FIG. 16. Eigenvalues of $m/n=2/1$ double tearing modes in reversed magnetic shear plasmas with $\eta=10^{-8}$, normalized by eigenvalues obtained without numerical matching technique, as a function of $q_{\rm min}$ and the inner region width Δr. As $q_{\rm min}$ becomes closer to 2, $\gamma_{\rm global}$ itself approaches 0, and therefore $\gamma/\gamma_{\rm global}$ takes a rather large value. The distance between $q=2$ surfaces for $q_{\rm min}=1.9$ is about 0.1, which is the reason of large errors for $\Delta r=0.1$ in the range of $q_{\rm min}\leq 1.92$.

3/5, depending on the distance between the two mode-resonant surfaces Δr_s. When Δr_s is small, $x\simeq 1/3$, and the mode has the double tearing type structure. On the other hand, $x\simeq 3/5$ when Δr_s is large, and the mode has something like two single tearing type structure. As for our calculation results, the mode structure was double tearing type even for $\eta=10^{-12}$. Thus, the dependence $\gamma\propto\eta^{1/3}$ approximately is reasonable. We mention that the magnitude of γ as well as the same η dependence was obtained by using the numerical matching technique for wide range of η.

Figure 16 shows the growth rate for $\eta=10^{-8}$, normalized by the growth rate obtained without the numerical matching technique, as a function of $q_{\rm min}$. In the range of $1.94\leq q_{\rm min}<2$, no dependence on Δr is observed; it means that $\Delta r=0.1$ is wide enough for the equilibrium parameters used for these calculations. Actually, if we try to define a resistive-layer width x_r for a case of $q_{\rm min}$ being a rational number and $q'=0$ there, $x_r:=|2r/nB_\theta q''|^{1/4}\eta^{1/4}$ evaluated at the rational surface. This is obtained by taking a balance of terms in the low-beta reduced MHD equation around the rational surface. Then, $x_r=0.0037$ in this case. Therefore, $\Delta r=0.1$ means $\Delta r/x_r=27$, which is sufficiently large. As $q_{\rm min}$ becomes closer to 2, we observe the increase in $\gamma/\gamma_{\rm global}$ above unity, although it is still of the order of 1%. This is because that $\gamma_{\rm global}$ itself goes to 0 as $q_{\rm min}$ goes to 2, and thus it is difficult to keep numerical accuracy. If the growth rate is not so close to 0 even for $q_{\rm min}=2$ by taking account of finite pressure effect, for example, a good numerical accuracy is obtained. A good convergence cannot be obtained if the two $q=2$ surfaces are located so close to the boundaries r_L and r_R. For $q_{\rm min}=1.9$, the distance between two $q=2$ surfaces is about 0.1, which is the reason of the large errors for $\Delta r=0.1$ in the range of $q_{\rm min}\leq 1.92$. In this situation, it is better to locate two inner regions at the two $q=2$ surfaces and to match these solutions onto the solutions in the three ideal MHD regions.

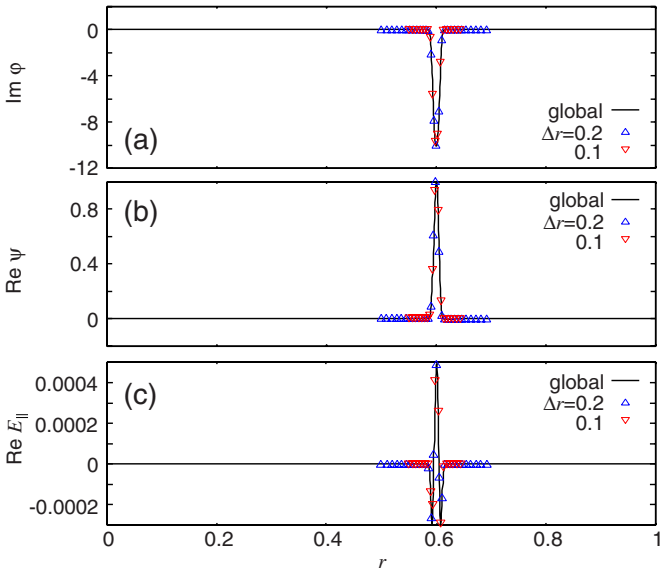

FIG. 17. (Color online) Eigenfunctions of $m/n=2/1$ double tearing modes in reversed magnetic shear plasmas with $q_{\rm min}=1.999$ and $\eta=10^{-8}$. (a) Imaginary part of φ, (b) real part of ψ, and (c) real part of $E_\parallel$. We find good agreement between the eigenfunctions with and without our numerical matching technique.

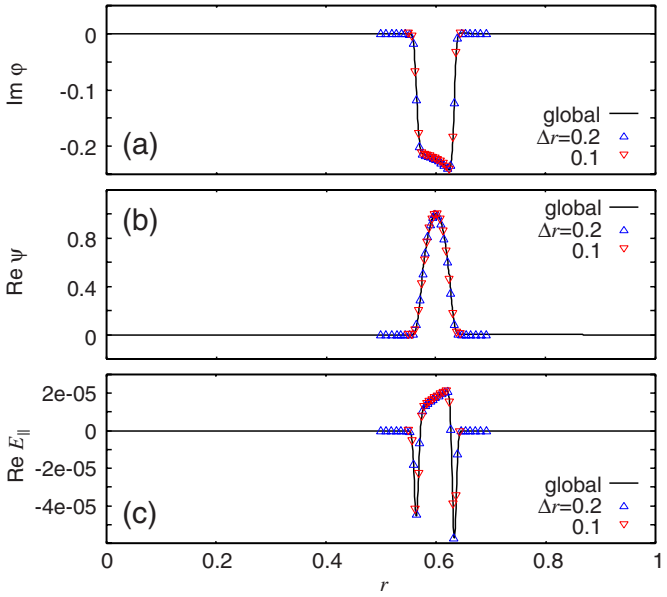

FIG. 18. (Color online) Eigenfunctions of $m/n=2/1$ double tearing modes in reversed magnetic shear plasmas with $q_{\rm min}=1.95$ and $\eta=10^{-8}$. (a) Imaginary part of φ, (b) real part of ψ, and (c) real part of $E_\parallel$. We find good agreement between the eigenfunctions with and without our numerical matching technique.

Figures 17 and 18 show the eigenfunctions for $q_{\rm min}=1.999$ and 1.95, respectively. The parallel electric field $E_\parallel$ was calculated by using the eigenfunctions φ and ψ. The eigenfunctions in the inner region obtained by the numerical matching are overlaid on the eigenfunctions by the global calculation (without the matching). Good agreement with the global calculation is obtained.

III. LINEAR INITIAL-VALUE PROBLEM

A. Settings

In this section, the numerical matching technique is applied to the calculation of the tearing mode stability via an initial-value problem. The setting of the problem such as the aspect ratio is the same as in Sec. II for the eigenvalue problem.

B. Outer region

In the outer region, we solve the Newcomb equation (13) to obtain the Green's function as in the eigenvalue problem. Then we express the solutions as

$$\psi_{\mathrm{out,L}}(r,t) = \psi_{\mathrm{L}}(t) G_{\mathrm{out,L}}(r) \tag{43}$$

for $0 \le r \le r_{\mathrm{L}}$, and

$$\psi_{\mathrm{out,R}}(r,t) = \psi_{\mathrm{R}}(t) G_{\mathrm{out,R}}(r) \tag{44}$$

for $r_{\mathrm{R}} \le r \le 1$. They are different from the expressions for the eigenvalue problems (16) and (19) so that the amplitude coefficients ψ_{L} and ψ_{R} are considered to be time dependent. This assumption may not be trivial, in general. However, if $\psi_{\mathrm{out,L}}(r,t)$ and $\psi_{\mathrm{out,R}}(r,t)$ are substituted into the linearized MHD equations, the time-derivative terms can be neglected in the outer region since we are focusing on slow resistive modes. Then $\psi_{\mathrm{out,L}}(r,t)$ and $\psi_{\mathrm{out,R}}(r,t)$ satisfy the Newcomb equation approximately.

C. Inner region

We solve the linearized reduced MHD equations

$$\frac{\partial}{\partial t}\begin{pmatrix} \nabla_\perp^2 & 0 & 0 \\ 0 & 1 & 0 \\ 0 & 0 & 1 \end{pmatrix}\begin{pmatrix} \varphi \\ \psi \\ p \end{pmatrix} = \begin{pmatrix} 0 & -\left(\mathrm{i}n\varepsilon - \dfrac{\mathrm{i}m\psi_0'}{r}\right)\nabla_\perp^2 - \dfrac{\mathrm{i}mJ_0'}{r} & \dfrac{\mathrm{i}m\kappa_{0r}}{r} \\ -\left(\mathrm{i}n\varepsilon - \dfrac{\mathrm{i}m\psi_0'}{r}\right) & \eta\nabla_\perp^2 & 0 \\ \dfrac{\mathrm{i}m\beta'}{r} & 0 & 0 \end{pmatrix}\begin{pmatrix} \varphi \\ \psi \\ p \end{pmatrix}, \tag{45}$$

as an initial-value problem in the inner region. Equilibrium flows are assumed to be zero. The above equations are not the so-called inner-layer equation with an expanded radial coordinate and frequency.

In order to solve the evolution equation, we adopt the implicit method. If φ, ψ, p, and t at the ith time step are denoted by φ^i, ψ^i, p^i, and t^i, respectively, we obtain the following difference equations:

$$(\nabla_\perp^2\varphi)^{i+1} - \Delta t\left[-\left(\mathrm{i}n\varepsilon - \frac{\mathrm{i}m\psi_0'}{r}\right)(\nabla_\perp^2\psi)^{i+1} - \frac{\mathrm{i}mJ_0'}{r}\psi^{i+1} + \frac{\mathrm{i}m\kappa_{0r}}{r}p^{i+1}\right] = (\nabla_\perp^2\varphi)^i, \tag{46}$$

$$\psi^{i+1} - \Delta t\left[-\left(\mathrm{i}n\varepsilon - \frac{\mathrm{i}m\psi_0'}{r}\right)\varphi^{i+1} - \eta(\nabla_\perp^2\psi)^{i+1}\right] = \psi^i, \tag{47}$$

$$p^{i+1} - \Delta t\frac{\mathrm{i}m\beta'}{r}\varphi^{i+1} = p^i, \tag{48}$$

where Δt denotes the time step size.

In the inner region, we consider an inhomogeneous solution as well as Green's functions for the initial-value problem. The Green's functions are obtained by setting the right-hand side be zero in Eqs. (46)–(48). The boundary conditions (20) and (22) are imposed similar to the eigenvalue problem, and we obtain $\mathbf{G}_{\mathrm{in,L}}$ and $\mathbf{G}_{\mathrm{in,R}}$ for a given Δt. We need to be careful since the definition of these Green's functions is different from those in the eigenvalue problem.

The inhomogeneous solution is obtained by retaining the right-hand side of Eqs. (46)–(48). Let us denote $\mathbf{H} := {}^{\mathrm{t}}(\varphi, \psi, p)$ and impose the following boundary conditions:

$$\mathbf{H}_{\mathrm{in}}^{i+1}(r_{\mathrm{L}}) = \mathbf{H}_{\mathrm{in}}^{i+1}(r_{\mathrm{R}}) = \begin{pmatrix} * \\ 0 \\ - \end{pmatrix}. \tag{49}$$

The asterisk again denotes that Eq. (24) is imposed for φ and $-$ denotes that no boundary condition is imposed for p.

Then, the solution in the inner region can be expressed as

$$\begin{pmatrix} \varphi^{i+1} \\ \psi^{i+1} \\ p^{i+1} \end{pmatrix} = \psi_{\mathrm{L}}^{i+1}\mathbf{G}_{\mathrm{in,L}}(r) + \psi_{\mathrm{R}}^{i+1}\mathbf{G}_{\mathrm{in,R}}(r) + \mathbf{H}_{\mathrm{in}}^{i+1}(r). \tag{50}$$

Here, the amplitude coefficients ψ_{L}^{i+1} and ψ_{R}^{i+1} are chosen to be equal to $\psi_{\mathrm{L}}(t^{i+1})$ and $\psi_{\mathrm{R}}(t^{i+1})$ in the outer regions, respectively. This choice makes ψ continuous across the boundaries $r = r_{\mathrm{L}}$ and r_{R}.

In addition, we impose the continuity of $\partial\psi/\partial r$ across these boundaries. Writing the ψ components of $\mathbf{G}$ and $\mathbf{H}$ as G and H, respectively, we obtain

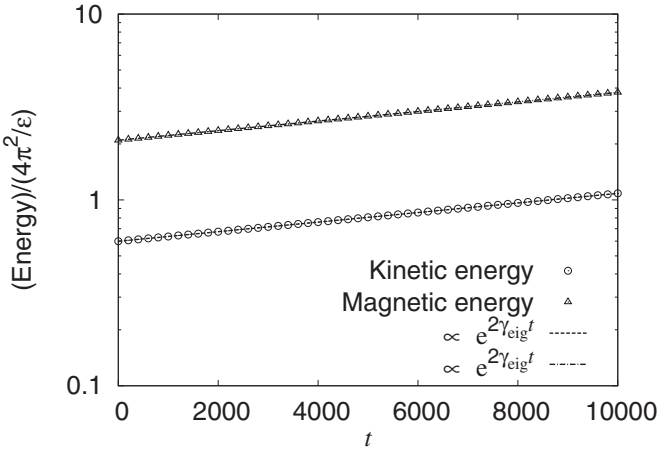

FIG. 19. Time evolution of kinetic and magnetic energy. As a reference, curves are plotted by using the eigenvalue obtained by the eigenvalue problem. Our numerical matching technique correctly capture the exponential growth via the initial-value approach.

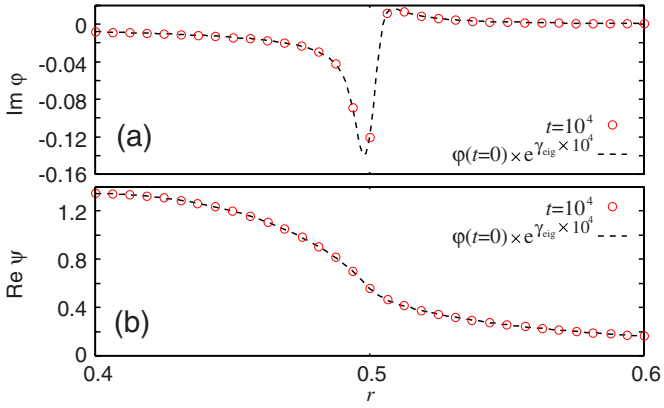

FIG. 20. (Color online) The mode structure at $t=10^4$ by the initial-value problem is shown. (a) Imaginary part of φ and (b) real part of ψ. The eigenfunctions obtained by the eigenvalue problem, or the initial condition, multiplied by the amplification factor $e^{\gamma_{eig}t}$ with the eigenvalue γ_{eig} and $t=10^4$, are plotted together. We find good agreement between them.

$$\begin{pmatrix} G'_{in,L}(r_L)-G'_{out,L}(r_L) & G'_{in,R}(r_L) \\ G'_{in,L}(r_R) & G'_{in,R}(r_R)-G'_{out,R}(r_R) \end{pmatrix} \begin{pmatrix} \psi_L^{i+1} \\ \psi_R^{i+1} \end{pmatrix} = -\begin{pmatrix} (H_{in}^{i+1})'(r_L) \\ (H_{in}^{i+1})'(r_R) \end{pmatrix}, \tag{51}$$

where the prime denotes radial derivative. By solving this equation, we obtain ψ_L^{i+1} and ψ_R^{i+1}.

Since this is a linear problem, we only need to solve for $\mathbf{G}_{in,L}$ and $\mathbf{G}_{in,R}$ only once at the beginning of the simulation if Δt is not changed. In addition, the matrix appearing in the left-hand side of Eqs. (46)–(48) does not change in time. Thus, we only need to LU decompose the matrix once at the beginning of the simulation. Then, the forward and backward substitutions are operated on the source term to obtain $\mathbf{H}_{in}^{i+1}$ at each time step.

D. Application

The numerical example shown in this subsection is for a zero-beta equilibrium with $j_t=j_{t0}(1-r^2)$, with j_{t0} determined such that $q_a=3.5$. The $m/n=2/1$ rational surface appears at $r=0.5$. Since the equilibrium pressure is assumed to be zero, the pressure equation (48) decouples from the others. For the results shown below, $\Delta r=0.2$ was used, although we also tried different values.

Figure 19 shows the time evolution of perturbed kinetic and magnetic energy for $\eta=10^{-8}$. The corresponding eigenfunction was used as the initial condition. Thus, we must observe the exponential growth with the corresponding growth rate. In the figure, curves proportional to $e^{2\gamma_{eig}t}$ are plotted together with the results of the time-evolution simulation, where γ_{eig} denotes the eigenvalue obtained by solving the corresponding eigenvalue problem. We observe that the obtained time evolution of energy is exactly what we expect.

Figure 20 shows the mode structure at $t=10^4$. As a reference, the eigenfunctions obtained by the eigenvalue problem, or the initial condition multiplied by the amplification factor $e^{\gamma_{eig}t}$ with the eigenvalue γ_{eig} and $t=10^4$, are plotted together. Figures 20 shows (a) the imaginary part of φ and (b) the real part of ψ. We observe good agreement between them, and they prove that the exponential growth of the mode is calculated correctly by our numerical matching technique.

IV. DISCUSSION

In this section, let us discuss the application of the present numerical matching technique to the stability calculation of high-beta plasmas in a toroidal geometry, which is one of the future issues of the extension of this study. The important differences between the cylindrical and the toroidal geometries are (i) the existence of nonresonant regular mode and (ii) the coupling between even and odd parity modes. As for item (i), we need to deal with the toroidal geometry actually. As for item (ii), such coupling of the parity can occur even in the cylindrical geometry if the resistivity is not so small. In the so-called inner-layer equation, there is no term which makes coupling between even and odd modes. This inner-layer equation is derived by taking the limit of infinitely small resistivity or thin layer. In this limit procedure, some terms which make coupling between even and odd modes are dropped in the governing equation. However, when the resistivity is not small and the "inner-layer," if we can define properly, is not thin, we cannot take such limit in the governing equation, and some terms remain finite, although they can be small, which can make coupling between even and odd parity modes. Some of the examples shown in the present paper dealt with such relatively large resistivity, and the numerical matching succeeds to capture the eigenmodes correctly. In addition, we have observed the uniform convergence property for different mode numbers for a range of resistivity, although the different mode numbers are decoupled in the cylindrical geometry. Therefore, we think that the application to the full toroidal finite-beta case is also possible.

V. CONCLUSIONS

We have developed a new numerical matching technique for the linear stability calculation of resistive MHD modes.

The solution to the resistive reduced MHD equations in an inner layer with *finite width* is matched onto the solution to the Newcomb equation. The boundary conditions adopted in the matching are the continuity of the stream function of magnetic field and its spatial derivative, and the smooth disappearance of parallel electric field. The latter is imposed as the boundary condition of the third kind for the stream function of velocity field. Since the number of independent solutions in the inner region (resistive MHD) and the outer regions (ideal MHD) are 4 and 2, respectively, the boundary conditions for the Green's functions in the inner region are chosen so that only two out of the four Green's functions can be matched onto the solutions in the outer region.

We have demonstrated that our matching technique is successfully applied to the linear stability calculations of tearing, internal kink, and resistive interchange modes in normal magnetic shear plasmas and double tearing mode in reversed magnetic shear plasmas in cylindrical geometry. Although we have not proved mathematically that the usage of the boundary condition explained above always leads to successful matching unfortunately, we showed that the boundary condition used in our matching technique is consistent with the conventional asymptotic matching solution in the limit of infinitely thin inner layer. Numerical examples of both eigenvalue and initial-value problems were shown. We found that good agreement is obtained among the results via the present matching technique and global solutions or results without using the matching technique. Our numerical matching technique is applicable to a wide range of resistivity, ranging from sufficiently small resistivity where the conventional asymptotic matching theory serves as a good approximation to large resistivity where the assumption for the conventional theory breaks down. For sufficiently small resistivity, we obtained good agreement of resistivity dependence of growth rates between our numerical results and the prediction by the conventional asymptotic matching theory. Even at large resistivity, our numerical matching theory is applicable, and we observed the deviation from the resistivity dependence given by the conventional asymptotic matching theory.

As mentioned in Sec. I, the advantages of utilizing the inner region with finite width are emphasized again: (i) this method can be used even if the Newcomb equation has an irregular singular point at the mode-resonant surface, i.e., reversed magnetic shear plasma with its minimum safety factor being a rational number; (ii) the Newcomb equation needs not to be integrated so close to the mode-resonant surface, which avoids special treatment of big solution and sensitive behavior of matching data on local MHD equilibrium accuracy and local grid arrangements around the mode-resonant surface; (iii) we do not need to care about the infinities of the stretched radial coordinate appearing in the conventional inner-layer equation and about the divergence of the norm of the solution; and (iv) this method can be easily applied to an initial-value problem. This feature can lead to study nonexponential behavior. We also expect that our method can provide a basis for an extension to study nonlinear phenomena. Application of more detailed inner-region equation may also be possible in the framework of the present numerical matching technique.

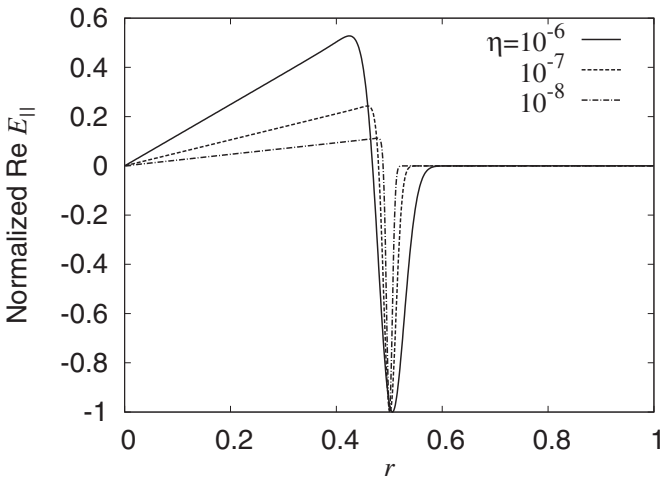

FIG. 21. The real part of the $E_{\|}$ is plotted for several values of η. The amplitude is normalized by each maximum value. The relative magnitude increases at $r<r_s$ as η is increased, which seems to be the reason why the matching does not give a good accuracy.

ACKNOWLEDGMENTS

This work was supported by Joint Institute for Fusion Theory (JIFT) exchange program and partly by Grant-in-Aid for Young Scientists (B) (Grant No. 19760595) from the Japan Society for the Promotion of Science (JSPS). A discussion with Dr. Y. Ishii at Japan Atomic Energy Agency was fruitful.

APPENDIX A: BOUNDARY CONDITION FOR *p*

When we include a heat diffusivity term $\chi\nabla_\perp^2 p$ on the right-hand side of the pressure equation, we need a boundary condition for p. This is obtained by the pressure equation and its radial derivative, as we did for the Ohm's law. The resultant boundary condition of the third kind is obtained as

$$\frac{\mathrm{d}p}{\mathrm{d}r} = -\frac{\varepsilon r\frac{n}{m}-\psi_0'}{\beta'} \times\left[-\frac{\beta''}{\varepsilon r\frac{n}{m}-\psi_0'}+\frac{\beta'\left(\varepsilon\frac{n}{m}-\psi_0''\right)}{\left(\varepsilon r\frac{n}{m}-\psi_0'\right)^2}-\frac{\beta'}{\varepsilon r\frac{n}{m}-\psi_0'}\frac{\psi'}{\psi}\right]p. \tag{A1}$$

When $\beta\equiv 0$, the pressure equation decouples from the other two equations. Therefore, we do not need to use this boundary condition.

APPENDIX B: *m*/*n*=1/1 INTERNAL KINK MODES WITH LARGE RESISTIVITY

As mentioned above, the numerical matching for large r_s, say $r_s=0.5$, with $r_L\neq 0$ does not give good accuracy especially when the resistivity is not sufficiently small. Figure 21 shows the parallel electric field $E_{\|}$ as a function of r, obtained by solving the linearized reduced MHD in the whole domain $0\leq r\leq 1$. The amplitude of $E_{\|}$ is normalized

such that the maximum absolute value becomes unity. The actual peak values of $E_{\|}$ are -1.33×10^{-4}, -3.03×10^{-5}, and -5.15×10^{-6} for $\eta=10^{-6}$, 10^{-7}, and 10^{-8}, respectively. We see that $E_{\|}$ at smaller r region has a relatively large value compared to that in the inner layer at $r=r_s=0.5$, especially when η is large. Since $E_{\|}$ does not disappear smoothly as going away from the mode-resonant surface, the numerical matching does not give a good accuracy in capturing this eigenmode. As η is decreased, we observe that the current sheet becomes sharper. We also understand that the conventional asymptotic matching method fails since there is no inner layer with infinitely thin width assumed in the theory. We may need to develop another boundary condition for this special case to obtain good accuracy.

[1]H. P. Furth, J. Killeen, and M. N. Rosenbluth, Phys. Fluids **6**, 459 (1963).
[2]B. Coppi, J. M. Greene, and J. L. Johnson, Nucl. Fusion **6**, 101 (1966).
[3]H. P. Furth, P. H. Rutherford, and H. Selberg, Phys. Fluids **16**, 1054 (1973).
[4]G. Ara, B. Basu, B. Coppi, G. Laval, M. N. Rosenbluth, and B. V. Waddell, Ann. Phys. (N.Y.) **112**, 443 (1978).
[5]A. Pletzer and R. L. Dewar, J. Plasma Phys. **45**, 427 (1991).
[6]M. S. Chu, R. L. Dewar, J. M. Greene, and A. Pletzer, Phys. Fluids B **5**, 1593 (1993).
[7]S. Tokuda and T. Watanabe, J. Plasma Fusion Res. **73**, 1141 (1997).
[8]J. W. Connor, S. C. Cowley, R. J. Hastie, T. C. Hender, A. Hood, and T. J. Martin, Phys. Fluids **31**, 577 (1988).
[9]A. Pletzer, A. Bondeson, and R. L. Dewar, J. Comput. Phys. **115**, 530 (1994).
[10]C. C. Hegna and J. D. Callen, Phys. Plasmas **1**, 2308 (1994).
[11]S. Tokuda, Nucl. Fusion **41**, 1037 (2001).
[12]W. A. Newcomb, Ann. Phys. (N.Y.) **10**, 232 (1960).
[13]J. P. Freidberg, *Ideal Magnetohydrodynamics* (Plenum, New York, 1987).
[14]S. Tokuda and T. Watanabe, Phys. Plasmas **6**, 3012 (1999).
[15]L.-J. Zheng and M. Kotschenreuther, J. Comput. Phys. **211**, 748 (2006).
[16]A. H. Glasser, J. M. Greene, and J. L. Johnson, Phys. Fluids **18**, 875 (1975).
[17]A. H. Glasser, S. C. Jardin, and G. Tesauro, Phys. Fluids **27**, 1225 (1984).
[18]S. Tokuda and T. Watanabe, J. Plasma Fusion Res. **77**, 276 (2001).
[19]Y. Kagei and S. Tokuda, J. Plasma Fusion Res. **3**, 039 (2008).
[20]H. R. Strauss, Phys. Fluids **20**, 1354 (1977).
[21]R. D. Hazeltine and J. D. Meiss, *Plasma Confinement* (Dover, Mineola, NY, 2003).
[22]J. Shiraishi, S. Tokuda, and N. Aiba, Phys. Plasmas **17**, 012504 (2010).
[23]B. R. Suydam, Proceedings of the Second United Nations International Conference on the Peaceful Uses of Atomic Energy, 1959, Vol. 31, p. 157.
[24]J. Wesson, *Tokamaks* (Clarendon, Oxford, 2004).
[25]L. Zakharov and B. Rogers, Phys. Fluids B **4**, 3285 (1992).
[26]Y. Ishii, M. Azumi, G. Kurita, and T. Tuda, Phys. Plasmas **7**, 4477 (2000).